The Journal of Experimental Biology 208, 1445-1451
Published by The Company of Biologists 2005
doi:10.1242/jeb.01530

Propulsive force calculations in swimming frogs

II. Application of a vortex ring model to DPIV data

Eize J. Stamhuis[1,*] and Sandra Nauwelaerts[2]

[1]*Department of Marine Biology, University of Groningen, Biological Centre, PO Box 14, 9750 AA Haren, The Netherlands* and [2]*Department of Biology, University of Antwerp, campus 3 eiken, Universiteitsplein 1, B-2610 Wilrijk (Antwerpen), Belgium*

*Author for correspondence (e.j.stamhuis@biol.rug.nl)

Accepted 19 October 2004

Summary

Frogs propel themselves by kicking water backwards using a synchronised extension of their hind limbs and webbed feet. To understand this propulsion process, we quantified the water movements and displacements resulting from swimming in the green frog *Rana esculenta*, applying digital particle image velocimetry (DPIV) to the frog's wake.

The wake showed two vortex rings left behind by the two feet. The rings appeared to be elliptic in planform, urging for correction of the observed ring radii. The rings' long and short axes (average ratio 1.75:1) were about the same size as the length and width of the propelling frog foot and the ellipsoid mass of water accelerated with it. Average thrust forces were derived from the vortex rings, assuming all propulsive energy to be compiled in the rings. The calculated average forces (F_{av}=0.10±0.04 N) were in close agreement with our parallel study applying a momentum–impulse approach to water displacements during the leg extension phase.

We did not find any support for previously assumed propulsion enhancement mechanisms. The feet do not clap together at the end of the power stroke and no 'wedge-action' jetting is observed. Each foot accelerates its own water mantle, ending up in a separate vortex ring without interference by the other leg.

Key words: frog, *Rana esculenta*, swimming, thrust force, vortex ring, DPIV.

Introduction

Frogs swim by kicking water backwards with a synchronised extension of their hind limbs (Gray, 1968). The main forces acting during swimming are thrust from the backwards-moving webbed feet during the kick phase, and parasite drag on the forward-moving body during the kick as well as the retraction (glide) phase (Alexander, 2002; Nauwelaerts and Aerts, 2003). When looking at the overall swimming cycle, these forces should balance.

In the absence of methods to quantify water displacements and derive thrust forces directly, several modelling approaches have been used to map instantaneous propulsion throughout the kick-and-glide cycle in frogs and other self-propelling aquatic animals with a similar swimming style. These models were based on the thrust *vs* drag force balance that explained the movement of the centre of mass and were expressed in more general terms (e.g. Blake, 1981; Daniel, 1984, 1995) or with special application to frog swimming (e.g. Gal and Blake, 1988a,b; Nauwelaerts and Aerts, 2003). Thrust forces were estimated by considering the resistive forces of the flat propulsive structure(s) as well as the added mass of the water mantle carried along by propulsor. Refinements of the models were found in treating the propulsive structure as an array of elements that each contribute to propulsion autonomously ('blade element approach'), and in redefining the added mass volume (Blake, 1979; Morris et al., 1985; Stamhuis and Videler, 1998). With regard to frog swimming, differences between the centre of mass kinematics and the modelled hind limb forces were interpreted as deficits in thrust and were explained by assuming the existence of two additional thrust enhancing mechanisms: (1) interference between the two feet during leg extension, resulting in larger functional foot areas, and (2) backwards jetting of water when the two feet were forcefully brought together at the end of the power stroke (Gal and Blake, 1988b).

Validation of the existence of the suggested thrust and drag mechanisms and of the hydrodynamic models used to estimate the balancing forces can only be done by studying the flow phenomena involved in a quantitative way. Instantaneous quantitative information with good spatial resolution of the flow in the vicinity of swimming animals allows for analysis of the flow phenomena present during the propulsion generation phase as well as the flow patterns left behind in the wake (Stamhuis and Videler, 1995). In the accompanying paper, Nauwelaerts et al. (2005) studied the propulsion process

and force balance of swimming green frogs *Rana esculenta* during the leg extension phase, aiming at a comparison between terrestrial and aquatic locomotion in one species. They showed that it is possible to estimate the propulsive forces from multi-planar digital particle image velocimetry (DPIV) recordings and were able to derive a reliable force balance throughout the leg extension (kick) phase. Mapping of the flow during the whole kick phase does, however, put quite a constraint on the experimental conditions, because the frog has to swim exactly along a certain path in the illuminated plane (Nauwelaerts et al., 2005). Instead, flow phenomena in the wake, which are easier to map, may serve as propulsion estimators.

Quantitative analyses of wakes have been performed previously in flying birds (e.g. Spedding et al., 1984; Spedding, 1986, 1987; Spedding et al., 2003), in undulatory swimming fish (e.g. Blickhan et al., 1992; Müller et al., 1997) and in fish with pectoral fin propulsion (e.g. Drucker and Lauder, 1999). Detailed analysis of vortex rings present in the wakes allowed for the calculation of the impulse and energy stored in the rings, which could be used for the derivation of average propulsive force (Rayner, 1979a,b,c; Drucker and Lauder, 1999). So far, this approach has not been applied to frog swimming or any similar propulsory mode.

The aim of this paper is to verify the existence of alternative thrust-enhancing mechanisms in swimming frogs. Furthermore, the validity of a vortex ring approach as a method to calculate propulsive forces will be evaluated. Finally, average propulsive forces will be calculated based on hydrodynamic parameters in the vortex wake of swimming frogs. The results will be compared with propulsive force calculations from instantaneous–momentum development during active propulsion in frogs (Nauwelaerts et al., 2005).

Materials and methods

Animals and experimental conditions

Green frogs *Rana esculenta* L. (N=5, snout–vent length 0.05±0.01 m, mass 0.015±0.03 kg) were caught in the wild and housed in a glass terrarium (for details, see Nauwelaerts et al., 2005). Prior to the flow-mapping experiments, one frog at a time was introduced into the experimental glass aquarium (40 cm×15 cm×30 cm) containing fresh tapwater to a level of 14 cm. A Perspex raft (20 cm×14 cm) was floating on the surface to prevent the animals from swimming at the surface and to avoid image blurring by surface waves when taking video recordings in top view. The raft kept part of the surface uncovered, allowing the animals to pause and breathe at the water surface. Animals were startled by finger tapping on the aquarium or gently touching it, after which the frog swam a voluntarily chosen track towards the opposite side of the aquarium. The swimming speed was chosen by the frog. The recorded field of view was some distance from the starting point to ensure that we recorded the second or third kick. In total we recorded about 50 image series from five frogs. Only the sequences in which the animal extended both legs at the same time and swam a horizontal path with at least one of its feet moving through the (horizontal or vertical) laser sheet were used for further processing, therefore only ten sequences from two frogs, which we considered representative, were selected for analysis.

The water was seeded with neutrally buoyant Pliolite particles (BASF, Leverkusen, Germany) with a diameter of about 25 μm. Illumination was provided from the top or from the side by a laser light sheet of 0.2 mm thickness produced by a red light Krypton laser (Coherent Innova K, Coherent Lasers Inc, Santa Clara, CA, USA; λ=647 nm, P_{max}=1 W) provided with a cylindrical lens (f=10 mm), resulting in a vertical or horizontal light sheet. Illuminated areas of about 5 cm×5 cm in the swimming track of the frogs were imaged from the side as well as the top view using a high-speed video camera (Redlake MASD, Inc. San Diego, CA, USA) at 250 Hz, shuttered at 1/500 s. The camera was provided with a 5 mm macro ring and an aspherical Canon lens (f=50 mm, F=1.3) operated at maximum aperture. Image series including the swimming frogs during kick and retraction phase were analysed using a momentum–impulse approach, as presented in Nauwelaerts et al. (2005). Image series of the last part of the kick phase and of the remaining wake were analysed using a vortex-ring–momentum approach, as presented in this paper.

Flow analysis

Frame series of the illuminated particles in the wakes of the swimming frogs were analysed pairwise using a particle image velocimetry program (SWIFT 4.0, Dutch Vision Systems, Breda, The Netherlands). Image cross-correlation was performed with convolution filtering applying a 51×51 pixels interrogation area size and 65% overlap, and peaks were located using a COGW (centre of gravity weighed to grey value) method (Stamhuis et al., 2002). Average particle displacements in the jet and cohering vortex ring were in the order of magnitude of 1–6 pixels, and the displacement detection limit was below 0.05 pixels. Erroneous vectors and obvious outliers were removed in a manual validation procedure and replaced using 2D spline interpolation (Stamhuis and Videler, 1995; Stamhuis, 2005a). In general, maximally between 2 and 10 flow vectors were interpolated on a typical data set of 400 vectors. Calibration was performed by filming a Perspex grid prior to the experimental session.

PIV image cross correlation resulted in a velocity vector flow field of the imaged 2D plane with vectors arranged gridwise, allowing the derivation of the 2D distribution of the vorticity ω and the divergence θ, and the application of a vortex-locator d (discriminant for complex eigenvalues). These parameters aid in identifying and characterising flow phenomena, in particular vortices and vortex rings (Stamhuis and Videler, 1995; Müller et al., 1997). The distribution of the divergence θ was used to identify out-of-plane flow, indicating misalignment of laser sheet and jet flow direction and thereby potential underestimation of the velocity magnitude. Image series with substantial out-of-plane flow components were removed from the data sets. The distributions of velocity

magnitude, vorticity ω and the vortex locator *d* were used to identify vortices and vortex rings and estimate their morphometric characteristics. Cubic spline interpolation and graphic (colour coded) representation of these parameters were used to attain a higher morphometric accuracy and facilitate interpretation of the flow fields. Only those image sequences in which the laser sheet crossed the middle of the foot and thereby the middle plane of the resulting vortex ring were used for analysis, to prevent underestimation of the vortex ring momentum.

The velocity distributions of the vortex ring jets and vortices were mapped in the direction of the jet as well as perpendicular to the jet, and compared to expected theoretical velocity distributions (Milne-Thomson, 1966; Spedding et al., 1984; Spedding, 1987; Müller et al., 1997; Drucker and Lauder, 1999). This comparison served as a validity check for application of the vortex ring momentum calculation model (Rayner, 1979a,b,c; Spedding et al., 1984) (Fig. 1). Eventually, the ring momentum, derived from the circulation, is used to estimate average propulsive force.

Propulsive force estimation

The circulation Γ of the ring-shaped vortex was calculated from the closed-loop integration of the velocity component **v** in the direction of the jet main axis (Batchelor, 1967). For a vortex ring travelling through still fluid, this can be simplified to a line integral along the jet main axis (Spedding et al., 1984):

$$\Gamma = \oint \mathbf{v} dy' = \int_{-\infty}^{+\infty} \mathbf{v} dY' . \quad (1)$$

This again simplifies in practice to a line integration from upstream of the vortex ring where $\mathbf{v}\approx 0$ along the Y' axis to downstream of the vortex ring where again $\mathbf{v}\approx 0$:

$$\Gamma = \int_{-y'(\mathbf{v}\approx 0)}^{+y'(\mathbf{v}\approx 0)} \mathbf{v} dY' . \quad (2)$$

The momentum *I* present in the vortex ring can be obtained from the product of the fluid density ρ, the circulation Γ and the ring area calculated from its radius *R*:

$$I = \rho \Gamma \pi R^2 . \quad (3)$$

This momentum has been accumulated during the process of vortex ring formation, in this case the propulsion phase of the frog's leg(s). The average propulsive force can be calculated by dividing the accumulated momentum *I* by the propulsion phase period time *T*:

$$\bar{F} = \frac{I}{T} = \frac{\rho \Gamma \pi R^2}{T} . \quad (4)$$

The propulsion time *T* was derived from the propulsive phase history as the fraction of the leg extension phase that contributes positively to the propulsion. The extension phase could easily be determined from the leg kinematics. The propulsive fraction appeared to be 0.75±0.05 on average, that is 75% of the extension time (see Nauwelaerts et al., 2005).

Depending on the level of interference of both legs during the propulsive stroke, this propulsive force has to be corrected. The level of interference as well as the presence and contribution of alternative propulsion mechanisms such as wedge action of the feet will be estimated and evaluated from the PIV flow maps.

Results

Presence of alternative propulsion mechanisms

In ten of the recorded sequences, five in dorsal and five in lateral perspective, the frog was swimming along a path parallel to the illumination sheet with one or both of its feet in the sheet. We analysed these sequences in detail, to get a proper interpretation of the flow phenomena involved in frog swimming. Significant interference between the feet would theoretically have resulted in merging of the water masses around the individual feet. Significant wedge action at the end of the extension phase would theoretically have resulted in a jet caused by the water mass squeezed from the space between the feet. The DPIV flow maps of the last part of the propulsive stroke and of the wake present immediately after completion of the propulsive stroke did not show any evidence for either interference between the feet during the leg extension phase or wedge action of the feet when supposedly clapping together at the end of the propulsive stroke (Fig. 2). During the last part of the extension phase, each individual foot pushed an isolated volume of water backwards, without any indication of influence by the other foot (Fig. 2A). After completion of a propulsive stroke, two single vortex rings stayed behind, each originating from one of the two kicking legs (Fig. 2B). No 'clapping-jets' or other wedge action effects were visible in any of the analysed sequences. This indicates that the legs work as independent propulsors throughout the stroke cycle.

Vortex ring morphology and model validity

In total, seven swimming sequences from two animals out of the ten recordings that were selected based on swimming path, showed clearly recognisable vortex rings that had just been shed from one foot or both feet. These sequences were analysed to obtain vortex ring impulse momentum, five sequences showing a horizontal and two a vertical cross section of the wake. In five cases (three horizontal and two vertical), the propulsive part of one of the feet (mainly the toes) moved properly through the laser light sheet, giving a high probability that the ring was cross sectioned at or close to its centre by the light sheet. The vortex rings in the vertical cross section were difficult to map correctly, because the ring axes were hardly ever parallel to the laser sheet, resulting in relatively high out-of-plane flow components. This was due to the vortex ring jets left behind by the two feet being directed backwards but somewhat towards one another, allowing proper mapping in a horizontal plane but complicating vertical cross section mapping.

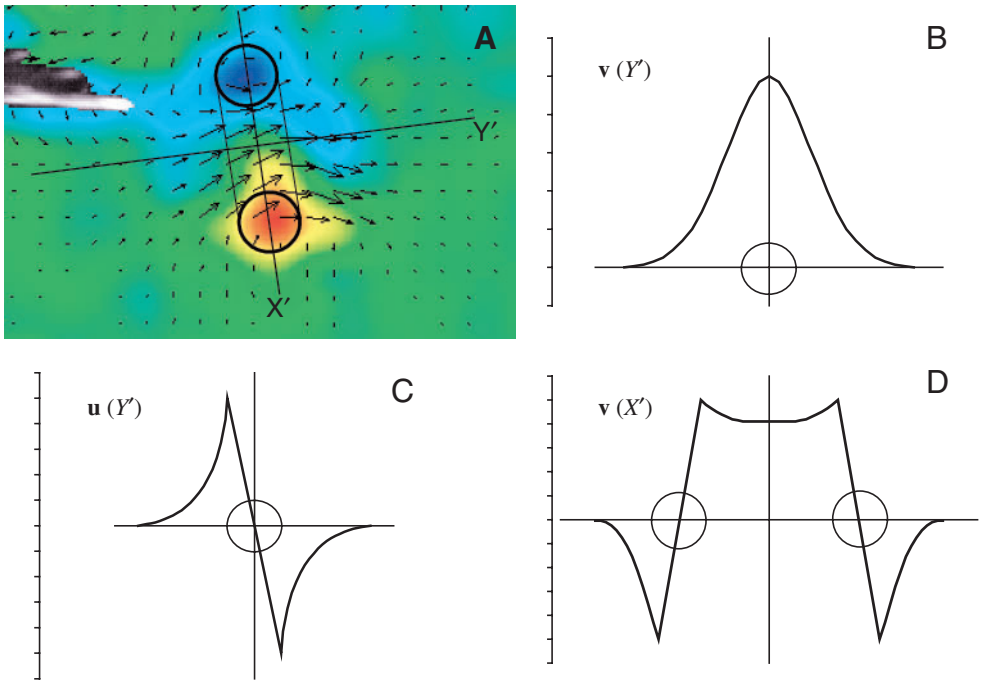

Fig. 1. Diagram of a vortex ring in cross section with the X' and Y' axes indicated, velocity components and velocity profiles. (A) Cross section of vortex ring left behind by the frog foot just disappearing on the left. Red, clockwise vorticity; blue, anti-clockwise vorticity; Y'-axis is normal to the vortex ring; X'-axis is perpendicular to the normal axis, parallel to the ring plane. (B) Predicted **v** velocity profile along the Y'-axis. (C) Predicted **u** velocity profile through vortex core along the Y'-axis. (D) Predicted **v** velocity profile along the X'-axis through both vortex cores.

The PIV recordings in lateral view (vertical cross section) showed vortex rings with significantly smaller diameter compared to the recordings in dorsal view (horizontal cross section) (Table 1) indicating the rings to be elliptic immediately after shedding. The vortex ring model assumes the rings to be circular and is quite sensitive to variation in the ring radius, determining the ring area (see equations 3 and 4). Therefore, we calculated a corrected ring radius based on cross sectional area πR^2 for a ring and πab for an ellipse, R being the ring radius and a and b being the half the short and long axis of the ellipse, respectively. The ring radius thus used for momentum calculations was $R=(ab)^{0.5}$. Because PIV analysis of the larger horizontally sectioned rings have a higher resolution with regard to spatial flow velocity distribution, and because of a higher probability of out-of-plane flow and thereby underestimation of the circulation in the vertically sectioned rings, we used the vertically sectioned rings to correct the ring radii of the horizontally sectioned rings, which were then used to derive impulse momentum and average propulsive forces. The measured ring radii from the horizontal sections had to be multiplied by 0.755±0.026 (± S.D.) to yield the corrected radii R.

All vortex rings used for impulse and force derivation showed the theoretically expected velocity distributions indicative for vortex rings, Fig. 3 serving as an example. In all cases, the jet velocity **v** along the X' axis showed a plateau-like distribution with typical zero crossings and velocity reversal in the vortices on both sides of the jet (Fig. 3A). The jet velocity **u** along the Y' axis showed a symmetrical profile with the peak in the middle of the ring (Fig. 3B). The velocity distribution along the Y' axis through the vortex centres showed reversal at the vortex centre; the velocity peaks at the edges of the core and decreases with distance outside of the core (Fig. 3C). These results matched the theoretical expectations, allowing momentum calculations from the vortex ring characteristics.

Vortex ring momentum and thrust force

The vortex ring characteristics and velocity distributions of

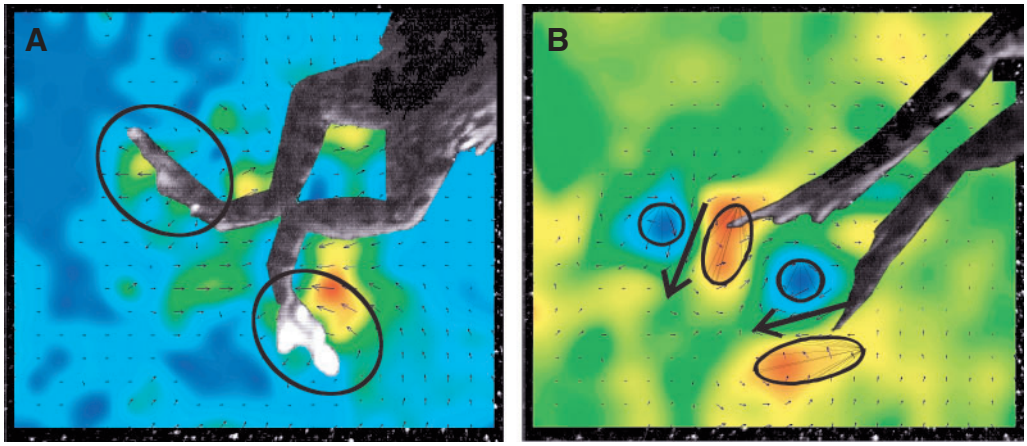

Fig. 2. Top views of a swimming frog during two successive stages of the kick cycle, illustrating the absence of assumed propulsion enhancement mechanisms. (A) Leg extension phase, showing rearward-directed flow around the webbed feet without mutual interference, indicated by the forward-directed flow inbetween (colour indicates flow magnitude, red=$\mathbf{v}_{max}\approx$0.66 m s^{-1}; blue≈0 m s^{-1}). (B) Just after completion of the extension phase showing two separate vortex rings, one from each leg (colour indicates vorticity ranging from –0.15 s^{-1}=blue to 0.15 s^{-1}=red).

Table 1. *Collection of all valid data from horizontal and vertical cross sections of frog-produced vortex rings, showing the parameters used to calculate thrust forces, and the final results*

Series	Frames	R (m)	R^* (m)	α (deg.)	$\mathbf{v}_{foot}$ (m s^{-1})	Circ. (m^2 s^{-1})	T (s)	T^* (s)	I (kg m s^{-1})	F_{foot} (N)	F_{tot} (N)
Horizontal											
k1s8c	44–45	0.0146	0.011023	14	0.54	0.00757	0.06	0.045	0.00289	0.0642	0.1284
	45–46	0.0162	0.012231	14	0.54	0.00805	0.06	0.045	0.00378	0.084	0.168
k3s7	75–76	0.0108	0.008154	12	0.35	0.00713	0.088	0.066	0.00149	0.0226	0.0452
	76–77	0.0131	0.009891	12	0.35	0.00672	0.088	0.066	0.00207	0.0314	0.0628
	77–78	0.0145	0.010948	12	0.35	0.00866	0.088	0.066	0.00326	0.0494	0.0988
k3s8b	53–54	0.0131	0.009891	34	0.51	0.00562	0.068	0.051	0.00173	0.0339	0.0678
	54–55	0.0145	0.010948	34	0.51	0.00876	0.068	0.051	0.0033	0.0647	0.1294
	55–56	0.014	0.01057	34	0.51	0.00775	0.068	0.051	0.00272	0.0533	0.1066
Vertical											
k1s4c	119–120	0.00465									
	120–121	0.00555									
k3s4b	99–100	0.00948									
	100–101	0.0094									

$F_{tot,av}$=0.101±0.041 (mean ± S.D.).

The horizontally sectioned rings were used for force derivation after radius correction using the vertically sectioned rings: R_{hor}=0.0128±0.0026); R_{vert}=0.0073±0.0025; $\rightarrow R^*$=0.0096±0.0026=0.755R_{hor}.

hor, horizontal; vert, vertical.

k1s8c, etc, series code containing frog number (k#), series number (s#) and shot indicator (a,b,c).

R, ring radius; R^*, corrected radius; α, angle of ring normal axis with mean swimming path; $\mathbf{v}_{foot}$, max. foot velocity during kick; Circ., circulation from intergral; T, extension time; T^*, propulsion time; I, ring momentum; F_{foot}=average propulsive force per foot; F_{tot}, total average propulsive force.

the horizontal cross-sections were sampled two or three times at 0.004 s interval from subsequent frame pairs. The results are summarized in Table 1. The circulation estimates showed very little variation between the samples as well as between shots and animals. The ring radii and the propulsive period time showed more variation, both between samples and between the animals. Because ring radius and propulsive period time appear as R^2/T in the thrust calculations, both are responsible for the variation in the calculated thrust forces, the radius to a higher degree than the period time.

The average total thrust force produced by both kicking legs of the swimming frogs was found to be 0.10±0.04 N. This is in close agreement with the average thrust forces derived from the force profiles in Nauwelaerts et al. (2005), being 0.12±0.05 N.

Most of the filmed sequences showed angles of 5–20° between the v' axis (normal axis of the ring) and the mean path of motion of the frogs. This indicates that normally more than 90% of the thrust force favours propulsion and that lateral forces are relatively small. This is again in good agreement with lateral force angle estimates of about 11° (Nauwelaerts et al., 2005). The angle of 34° found in one sequence shown in Table 1 was among the highest thrust angles found during all our experiments and is regarded as exceptional. It is most probably due to some lateral displacement of the foot for manoeuvring purposes just before ring was shed. Because all other characteristics of this sequence were in line with expectations and other results, there was no reason to exclude it from the data set.

Discussion

Thrust enhancement mechanisms

We did not find any evidence for interference of the two legs during the extension phase, nor for extra thrust from the feet clapping together at the end of the kick, as suggested by Gal and Blake (1988b). Improperly balancing forces as found by Gal and Blake (1988b) but also by Nauwelaerts and Aerts (2003) are more likely to be caused by overestimation of the drag on the body and subsequent adaptations of the model to accommodate for this (see discussion in Nauwelaerts et al., 2005). In our DPIV analyses, we always found water mantles that were accelerated with the individual foot without any connection with the water mantle of the other foot. The mantles were shed independently and showed up in the wake as independent vortex rings. In some cases, these vortex rings interfered or merged some time after they had been shed. This was, however, well after the propulsive phase had been completed and does not influence the thrust developed during the propulsion process itself. For comparison, we did perform some preliminary experiments with swimming clawed frogs *Xenopus laevis*, a fully aquatic species. This species showed

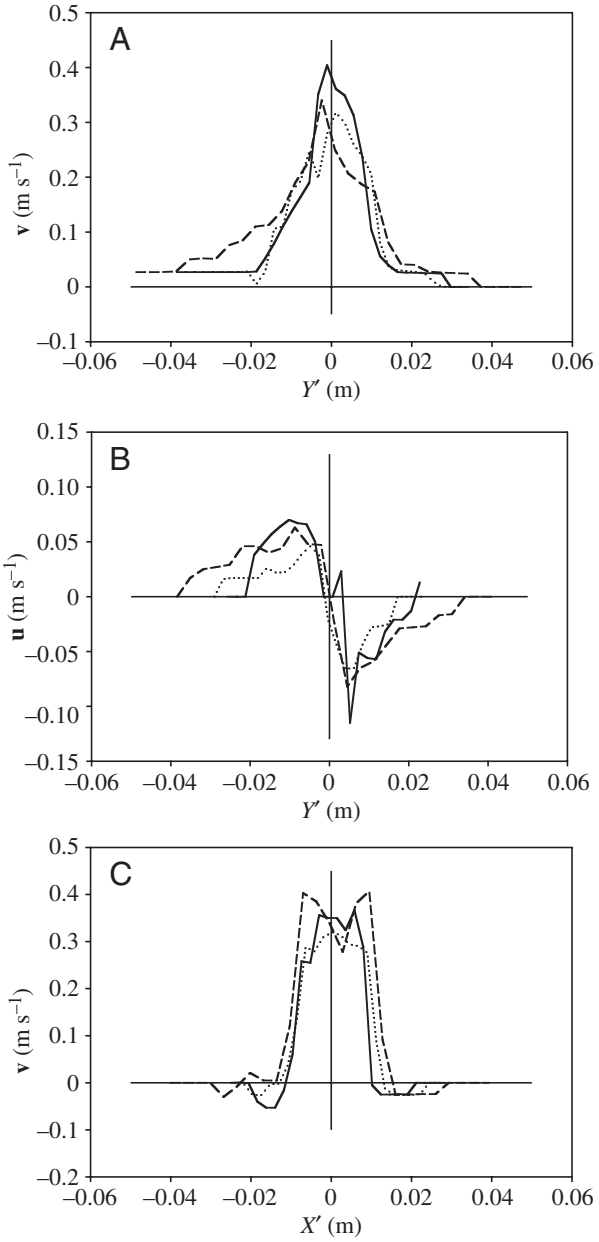

Fig. 3. Example graphs from vortex ring velocity profiles. (A) The velocity profile $\mathbf{v}(Y')$ of the jet along the normal axis of the vortex ring. (B) Velocity profile $\mathbf{u}(Y')$ through one of the vortex cores. (C) The velocity distribution $\mathbf{v}$ along the X' axis through the central jet and both vortex cores.

even more clearly that the two feet accelerate independent masses of water and leave behind two vortex rings that both travelled backwards or even somewhat away from one another. As in the green frog, there was no trace of jetting due to the feet clapping together (so-called 'wedge action'), which could have indicated additional thrust during the final stage of leg extension. With the naked eye, the feet seem to move towards one another at the end of the kick, but this should be interpreted as feathering to reduce drag during the first part of the gliding phase. This is in line with Nauwelaerts et al. (2005), who showed that no propulsion is produced during the last 20–30% of what is commonly interpreted as the kick phase (extension phase). We therefore conclude that acceleration of water masses due to the high resistance of the spread webbed feet during the kick phase is the sole mechanism of thrust production in swimming frogs.

An interesting parallel here is the kick phase of the human breast stroke. A few decades ago, the preferred motion pattern for the legs was 'retract-spread-and-close', with emphasis on closing as being an important source of thrust by stowing and squeezing water backwards (Counsilman, 1968). This technique is now outdated although still used in recreational swimming. The kick-phase with the feet only slightly open in a so-called 'W-bearing' to get a large area for backwards acceleration of water, is now widely accepted as the best propulsion style for human breaststroke. This technique is often referred to as 'Whip-action' when compared to the outdated 'Wedge-action' technique (Whitten, 1994). Swimming frogs apparently have a natural olympic swimming style, which humans seem to approach more and more regarding the leg technique for competitive breaststroke swimming.

Calculation of momentum from vortex rings.

The vortex rings left behind by the swimming frogs appeared to be elliptic. Nauwelaerts et al. (2005) showed the mass of water that moves with and is accelerated by the foot to be ellipsoid. Apparently, this causes the ring to be elliptic immediately after shedding, urging for correction of the ring radius to enable the application of momentum calculations through the vortex ring model. It may be possible that the vortex ellipse merges into a real ring shape in time. Nevertheless, we used the ellipse shaped ring immediately after shedding for impulse calculations because the energy in the vortex decreases rather steeply with time due to dissipation, and may be half of the original energy within tenths of a second (Müller et al., 1997; Stamhuis, 2005b). We trust our approach of radius correction of a recorded ring as short after shedding as possible to give the most reliable results.

The calculated forces based on the vortex ring model were about 20% lower than derived through an instantaneous impulse–momentum approach applied to water dragged along by the foot during the kick (Nauwelaerts et al., 2005). When comparing both methods within the same kick-cycle, which was possible for two of the recordings with two different frogs, the average forces match even better: 0.148 N *vs* 0.130 N (frog 1) and 0.069 N *vs* 0.082 N (frog 2) for the vortex ring *vs* the instantaneous impulse approach, respectively. This illustrates that both methods mutually support one another but also show some variation, probably due to the simplifications that were necessary when deriving forces for a 3D flow phenomenon from planar flow information. On average, the results for the vortex ring method were somewhat, but not statistically, significant (*t*-test, $P>0.2$), lower than the instantaneous impulse method, which may be explained by the fact that a vortex ring will practically never contain all the momentum from the

kicking foot, due to losses. Some energy will be lost at the interface of the water mass moving along with the foot during the kick and the surrounding water. Momentum or energy calculations derived from a vortex ring are therefore bound to underestimate the total energy that was invested to create the vortex ring. This was also concluded for momentum and energy derivations based on vortex rings created by a flying bird (Spedding, 1986) and swimming fish (Müller et al., 1997). We expect the losses to be less than 20% in the frog kick case, but realistic estimates are hard to derive at this stage. Most papers in the quite large body of literature on vortex ring phenomena examine the creation and evolution of vortex rings originating from pipes or nozzles (e.g. Schramm and Riethmuller, 2001; Shusser and Gharib, 2000). The creation of vortex rings by (flat) surfaces moving through free fluid, comparable to the frog kick, and the energetics during the vortex creation process, have had little attention so far. More theoretical as well as formalised experimental work would increase our understanding not only of frog swimming but also of other rowing propulsors.

In conclusion, derivation of thrust forces from the vortex rings in the wake of swimming green frogs seems a reliable way of estimating the average thrust force during the kick phase. Momentum derived from the vortex rings will be somewhat underestimated, but there is no indication that severe underestimation will take place. For reliable momentum calculations, the vortex ring should be cross-sectioned through its centre by the illumination sheet. Deviations from ring circularity should be corrected to avoid serious errors in the momentum estimations.

Peter Aerts (University of Antwerp) and John Videler (University of Graunjen) are kindly acknowledged for facilitating and stimulating the study presented here.

References

Alexander, R. McN. (2002). *Principles of Animal Locomotion*. Princeton/Oxford: Princeton University Press.

Batchelor, G. K. (1967). *An Introduction to Fluid Dynamics*. Cambridge: Cambridge University Press.

Blake, R. W. (1979). The mechanics of libriform locomotion. I. Labriform locomotion in the angelfish (*Petrophyllum eimekei*): an analysis of the power stroke. *J. Exp. Biol*. **82**, 255-271.

Blake, R. W. (1981). Drag-based mechanisms of propulsion in aquatic vertebrates. In *Vertebrate Locomotion*, *Symp. Zool. Soc. Lond*., Vol. 48 (ed. M. H. Day), pp. 29-53. London: Academic Press.

Blickhan, R., Krick, C., Zehren, D. and Nachtigall, W. (1992). Generation of a vortex chain in the wake of a subundulatory swimmer. *Naturwissenschaften* **79**, 220-221.

Counsilman, J. E. (1986). *The Science of Swimming*. Englewood Cliffs, NJ: Prentice-Hall, Inc.

Daniel, T. L. (1984). Unsteady aspects of animal locomotion. *Am. Zool.* **24**, 121-134.

Daniel, T. L. (1995). Invertebrate swimming: integrating internal and external mechanics. In *Biological Fluid Dynamics* (ed. C. P. Ellington and T. J. Pedley) pp. 61-89. Cambridge: The Company of Biologists.

Drucker, E. G. and Lauder, G. V. (1999). Locomotor forces on swimming fish: three-dimensional vortex wake dynamics quantified using digital particle image velocimetry. *J. Exp. Biol*. **202**, 2393-2412.

Gal, J. and Blake, R. W. (1988a). Biomechanics of frog swimming. I. Estimation of the propulsive force generated by *Hymenochirus boettgeri*. *J. Exp. Biol*. **138**, 399-411.

Gal, J. and Blake, R. W. (1988b). Biomechanics of frog swimming. II. Mechanics of the limb beat cycle in *Hymenochirus boettgeri*. *J. Exp. Biol*. **138**, 413-429.

Gray, J. (1968). *Animal Locomotion*. London: Weidenfeld and Nicolson.

Milne-Thomson, L. M. (1966). *Theoretical Aerodynamics*. New York: Macmillan Press.

Morris, M. J., Gust, G. and Torres, J. J. (1985). Propulsion efficiency and cost of transport for copepods: a hydromechanical model of crustacean swimming. *Mar. Biol*. **86**, 283-295.

Müller, U. K., van den Heuvel, B. L. E., Stamhuis, E. J. and Videler, J. J. (1997). Fish foot prints: morphology and energetics of the wake behind a continuously swimming mullet (*Chelon labrosus* Risso). *J. Exp. Biol*. **200**, 2893-2906.

Nauwelaerts, S. and Aerts, P. (2003). Propulsive impulse as a covarying performance measure in the comparison of the kinematics of swimming and jumping in frogs. *J. Exp. Biol*. **206**, 4341-4351.

Nauwelaerts, S., Stamhuis, E. and Aerts, P. (2005). Propulsive force calculations in swimming frogs. I. A momentum-impulse approach. *J. Exp. Biol*. **208**, 1435-1443.

Rayner, J. M. V. (1979a). A new approach to animal flight mechanics. *J. Exp. Biol*. **80**, 17-54.

Rayner, J. M. V. (1979b). A vortex theory of animal flight. Part 1, The vortex wake of a hovering animal. *J. Fluid Mech*. **91**, 697-730.

Rayner, J. M. V. (1979c). A vortex theory of animal flight. Part 2, The forward flight of birds. *J. Fluid Mech*. **91**, 731-763.

Schramm, C. and Riethmuller, M. L. (2001). Vortex ring evolution in an impulsively started jet using digital particle image velocimetry and continuous wavelet analysis. *Meas. Sci. Technol*. **12**, 1413-1421.

Shusser, M. and Gharib, M. (2000). Energy and velocity of a forming vortex ring. *Phys. Fluids* **12,** 618-621.

Spedding, G. R. (1986). The wake of a jackdaw (*Corvus monedula*) in slow flight. *J. Exp. Biol*. **125**, 287-307.

Spedding, G. R. (1987). The wake of a kestrel (*Falco tinnunculus*) in flapping flight. *J. Exp. Biol.* **127**, 59-78.

Spedding, G. R., Rayner, J. M. V. and Pennycuick, C. J. (1984). Momentum and energy in the wake of a pigeon (*Columba livia*) in slow flight. *J. Exp. Biol*. **111**, 81-102.

Spedding, G. R., Rosén, M. and Hedenström, A. (2003). A family of vortex wakes generated by a thrush nightingale in free flight in a wind tunnel over its entire range of flight speeds. *J. Exp. Biol.* **206**, 2313-2344.

Stamhuis, E. J. (2005a). Basics and principles of particle image velocimetry (PIV) for mapping biogenic and biologically relevant flows. *J. Aquat. Ecol*., in press.

Stamhuis, E. J. (2005b). Vortices rule the wake: structure and Reynolds' scaling of animal generated wakes. In *Flow Phenomena in Nature, A Challenge for Engineering Design* (ed. R. Liebe). Wessex Institute of Technology Press (in press).

Stamhuis, E. J. and Videler, J. J. (1995). Quantitative flow analysis around aquatic animals using laser sheet particle image velocimetry. *J. Exp. Biol*. **198**, 283-294.

Stamhuis, E. J. and Videler, J. J. (1998). Burrow ventilation in the tube dwelling shrimp *Callianassa subterranea* (Decapoda, Thalassinidea). III: Hydrodynamic modelling and the energetics of pleopod pumping. *J. Exp. Biol*. **201**, 2171-2181.

Stamhuis, E. J., Videler, J. J., Duren, L. A. and Müller, U. K. (2002). Applying digital particle image velocimetry to animal generated flows: Traps, hurdles and cures in mapping steady and unsteady flow in Re regimes between 10^{-2} and 10^{5}. *Exp. Fluids* **33**, 801-813.

Whitten, Ph. (1994). *The Complete Book of Swimming*. New York: Random House Inc.